Journal of Interdisciplinary Mathematics
ISSN: 0972-0502 (Print), ISSN: 2169-012X (Online)
DOI : 10.47974/JIM-2335

Mathematical modeling and numerical analysis of dynamic behavior in lubricated mechanisms : Case of Reynolds equation

Youssef Essadaoui [†]
Lab LaMDa
Department of Mathematics and Informatics
Ecole Nationale des Sciences Appliquées
Sultan Moulay Slimane University
Khouribga 40000
Morocco

Amine Laghrib *
Department of Mathematics and Informatics
LaMDa Laboratory
Ecole Nationale des Sciences Appliquées
Sultan Moulay Slimane University
Khouribga 40000
Morocco

Imad Hafidi [§]
Lab LIPIM
Department of Mathematics and Informatics
Ecole Nationale des Sciences Appliquées
Sultan Moulay Slimane University
Khouribga 40000
Morocco

Abstract

In this paper, we investigate the dynamic behavior of a lubricated mechanism in the incompressible case. The goal is to develop a mathematical model that describes the motion of the upper surface, based on the quasi-stationary Reynolds equation and Newton's second law. We also analyze the existence and uniqueness of solutions to the resulting differential equations, as well as the conditions under which global nonexistence of solutions may arise. Furthermore, we conduct a thorough numerical analysis of the parameters a and p,

[†] *E-mail:* youssefessadaoui2017@gmail.com
* *E-mail:* a.laghrib@usms.ma (Corresponding Author)
[§] *E-mail:* i.hafidi@usms.ma

examining their influence on the system's behavior. The results provide valuable insights into the dynamics of lubrication, enhancing the understanding of these mechanisms in practical applications.

Subject Classification: *Primary 49M05, Secondary 53C35.*

Keywords: *Lubricated mechanism, Quasistationary PDE, Reynolds equation.*

1. Introduction

Lubricated contacts are commonly used in mechanical systems composed of closely spaced solids in relative motion. Introducing a lubricating fluid into the space between these solids prevents direct solid-to-solid contact, which could otherwise damage the surfaces. This process reduces friction and passive resistance, thereby lowering stress and forces on the system. Furthermore, lubrication improves machine efficiency, conserves energy, and protects components from corrosion and wear, significantly extending their longevity. The lubricant employed can take the form of a nearly incompressible liquid like oil or water, commonly used in hydrodynamic bearings and thrust bearings. Alternatively, it may involve air, which necessitates accounting for compressibility effects in applications such as read heads, magnetic tapes, or aerodynamic bearings [1].

The Reynolds equation describes the behavior of thin fluid films, particularly in the context of lubrication theory [2, 3, 4]. This equation is fundamental for understanding fluid flow in narrow gaps or thin layers where viscous forces dominate. Its versatility extends across various fields, providing critical insights into engineering, manufacturing, and biological systems. Below are key applications: Hydrodynamic Bearings: The equation is extensively used to design and analyse hydrodynamic journal and thrust bearings that support rotating machinery. By calculating the pressure distribution within the fluid film, engineers can determine the load-carrying capacity of these bearings, ensuring smooth operation and longevity of mechanical systems [5, 6]. Microfluidics and Lab-on-a-Chip Devices: In microfluidics, where liquids flow through extremely narrow channels, the Reynolds equation guides the design of devices for applications such as DNA sequencing, chemical synthesis, and medical diagnostics. It provides insights into flow dynamics crucial for optimizing performance in these cutting-edge technologies [7]. Coating Processes: The manufacturing industry relies on the Reynolds equation to model the flow and distribution of coating fluids. This is essential in processes such as painting, printing, and the production of thin polymer films, ensuring uniform application and precise control over film thickness [8, 9]. Tribology and Contact Mechanics: Tribology, the study of friction, lubrication, and wear, leverages this equation to investigate lubrication performance in moving mechanical components like gears and seals. The pressure field derived from the Reynolds equation predicts film thickness and pressure buildup at contact points, reducing wear and enhancing efficiency [10]. In addition to its use in industrial applications, the Reynolds equation is also employed in biological systems to model fluid flow

within thin biological films, such as mucus in the lungs or synovial fluid in joints [11]. This application aids researchers in understanding and predicting the dynamics of these vital biological processes [12].

Various studies have contributed to the advancement of mathematical modelling techniques for the Reynolds equation in hydrodynamic lubrication, integrating modern computational methods and addressing complex phenomena such as cavitation. In [13], the authors present a deep learning computational framework, named HL-nets, which utilizes physics-informed neural networks (PINNs) to solve the Reynolds equation. This framework incorporates cavitation effects through classical conditions such as the Swift-Stieber and Jakobsson-Floberg-Olsson models. The study demonstrates that HL-nets can effectively and accurately simulate hydrodynamic lubrication phenomena, including cavitation.

The system in [14], associated with the equilibrium solution for the unknowns $(p, a, \theta) \in H_0^1(\Omega) \times \mathbb{R} \times \mathbb{R}$, is described by the following set of equations:

$$\begin{cases} \nabla \cdot [(h_0 + a + \theta x_1)^3 \nabla p] = \frac{\partial h_0}{\partial x_1} + \theta & \text{in}\Omega, \\ p = 0 & \text{on } \partial\Omega, \\ \int_\Omega p \, dx = F, \\ \int_\Omega p(x_1 - x_1^0) \, dx = 0. \end{cases} \tag{1}$$

where $h_0 : \Omega \to \mathbb{R}$ represents a given function that describes the shape of the slider's surface.

In all these applications, the terms $a(t)$ and $h_0(x)$ account for temporal and spatial variations in film thickness or surface topology, while the pressure field p provides insight into the mechanical effects of the fluid on the surrounding surfaces. The lubricated system examined in this work involves two nonparallel surfaces in hydrodynamic contact, a configuration that, to the best of our knowledge, has not been previously studied. The lower surface is assumed to be flat, horizontal, and in constant horizontal motion. Specific conditions are imposed on h_0 to ensure that $\int_\Omega p \, dx$ increases significantly as the gap between the surfaces narrows.

It is worth noting that, in a different context, the authors in [14] investigated the asymptotic behavior of solutions to equation (1) as the minimum value of h approaches zero. In [15], the dynamic problem described by (1), with a single degree of freedom, specifically the vertical displacement a was analyzed. The study established the existence and local uniqueness of a within the space $C^\infty([0, T_{\max}))$, while also providing conditions that ensure either global existence or its failure. These findings significantly advanced the understanding of dynamic systems, utilizing both classical analytical and numerical techniques.

Building on these theoretical insights, we propose a numerical analysis of the Reynolds equation using a finite volume scheme. The finite volume method is particularly well-suited for solving partial differential equations in complex

geometries, such as those encountered in hydrodynamic lubrication problems, as it ensures the conservation of fluxes and is robust in handling discontinuities or sharp gradients, which are common in lubrication flows. To discretize the Reynolds equation, we first partition the computational domain Ω into a finite number of control volumes. Each control volume corresponds to a cell in the discretized grid. The solution for the pressure field p is approximated at the center of each control volume, and the fluxes across the boundaries of each control volume are computed based on the numerical scheme.

The governing equation is then integrated over each control volume. For instance, for a 2D problem in a rectangular domain, the Reynolds equation can be expressed in integral form over each control volume C_i as:

$$\int_{C_i} \nabla \cdot [(h_0 + a + \theta x_1)^3 \nabla p]\, dA = \int_{C_i} \left(\frac{\partial h_0}{\partial x_1} + \theta\right)\, dA.$$

In 2D problems, dA corresponds to an infinitesimal area in the plane. If the domain Ω is a region in the x_1-x_2 plane, then dA is the area element, typically written as $dx_1\, dx_2$ in Cartesian coordinates. It represents the area of the control volume over which the integration is performed. Using the divergence theorem, this equation can be rewritten as a sum of fluxes across the control volume boundaries. The fluxes are approximated using a suitable numerical flux function, ensuring that the solution respects the physical properties of the system, such as conservation of mass and energy. The pressure field p is updated iteratively at each time step, while the other unknowns, such as a and θ, are treated as parameters or solved using appropriate numerical methods, depending on the system's dynamics. To handle the boundary conditions, a combination of Dirichlet and integral constraints (as specified in the problem) is applied at the appropriate boundaries of the computational domain.

The finite volume scheme can also be coupled with techniques such as adaptive meshing, where the resolution of the grid is refined in regions with steep gradients or high variations in pressure [16, 17]. This ensures greater accuracy in capturing the fluid dynamics, especially in the proximity of the narrow gap between the surfaces, where significant changes in the pressure field are expected [18]. The numerical solution provides detailed insight into the behavior of the fluid film, allowing for the prediction of lubrication performance, the study of cavitation effects, and the optimization of surface design in practical engineering applications.

The main paper is organized as follows. Section 2 presents the proposed model, along with an analysis of the asymptotic behavior of the Reynolds equation, including results on global existence and stability of the solution. Section 3 provides insights into the behavior of the variational equation. Section 4 focuses on the discretization approach and presents numerical results, including both one-dimensional and two-dimensional cases, as well as the evolutionary Reynolds equation. Finally, Section 5 is devoted to real-world applications, and the paper concludes with a summary in the final section.

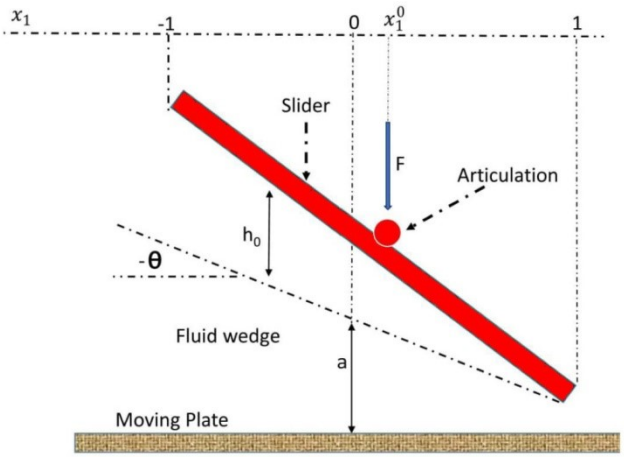

Figure 1
An illustrative example of a lubricated system consisting of a flat lower surface.

2. Asymptotic behavior of the Reynolds equation

For general shapes of the upper surface, there is limited literature on articulated sliders, with the exception of the one-dimensional planar case and a few scattered numerical results for specific instances. In [5], the authors aim to investigate the existence of equilibria for articulated sliders with arbitrary shapes described by $h(x) = h_0(x) + a + \theta x_1$. The normalized fluid pressure is independent of the surface normal and satisfies the Reynolds equation [19]:

$$\begin{cases} \nabla \cdot [h^3(x,t)\rho\nabla p] = \partial_{x_1}(\rho h) + \partial_t(h\rho) & x = (x_1, x_2) \in \Omega, t \geq 0 \\ p(x,t) = p_a \geq 0 & x \in \partial\Omega, \quad t \geq 0 \end{cases} \tag{2}$$

where $\Omega \subset \mathbb{R}^2$ is the projection of the domain containing the lubricant onto one of the surfaces. $h: \Omega \times [0, +\infty[\to \mathbb{R}^+$ represents the normalized thickness of the lubricating film, and ρ is the mass volumetric and $p = p(x,t)$ represents the fluid pressure. In this part, we consider the case of a lubricated system consisting of a flat lower surface (located in the horizontal plane) in uniform shear motion relative to an upper surface whose height is defined by $h(x,t)$ (see Figure 1). The fluid is assumed to be incompressible.

The upper surface is mobile and subjected to a constant vertical force $F > 0$. The lower surface, assumed to be flat and horizontal, is moving with a constant horizontal translation speed, as described in [20, 21]. Due to its motion, the lower surface drags the lubricant, which generates a pressure field opposing the applied force F. The upper surface is constrained to a single degree of freedom, namely its vertical displacement $a = a(t)$. The pressure $p = p(x,t)$ in the fluid satisfies the quasistationary Reynolds equation, which is typically expressed as:

$$\begin{cases} \nabla \cdot [(a(t) + h_0(x))^3 \nabla p] = a'(t) + \frac{\partial h_0}{\partial x_1} & \text{in } \Omega \\ p = 0 & \text{on } \partial\Omega \end{cases} \tag{3}$$

The motion of the upper surface is modelled by Newton's second law:

$$\begin{cases} a'' = \int_\Omega p \mathrm{dx} - F \\ a(0) = a_1^0 \\ a'(0) = a_2^0 \end{cases} \tag{4}$$

We assume that $\Omega^+ = \{x \in \Omega \ / \ p(x,t) > 0\}$, and h_0 verifies the following hypothesis:

$$\begin{cases} h_0 \in W^{1,\infty}(\Omega) \\ \min\limits_{x\in\Omega} h_0(x) = 0 \end{cases}$$

We are therefore seeking a solution where $a(t) > 0$ and $p(x,t)$ satisfy the system of equations given by problem (3)-(4). By linearity, the problem (3) can be reformulated as an ordinary differential equation of second order, which takes the form of a Lienard equation:

$$a''(t) = -g_2(a(t))a'(t) + g_1(a(t)) - F, \tag{5}$$

with conditions at time $t = 0$:

$$\begin{cases} a(0) = a_1^0 \\ a'(0) = a_2^0 \end{cases}$$

Where the functions g_i are defined for all $a > 0$ by :

$$g_i(a) = \int_\Omega p_i(x)dx \quad \mathrm{i} = 1,2,$$

where p_1 is the solution of:

$$\begin{cases} \nabla \cdot [(a + h_0(x))^3 \nabla p_1] = \frac{\partial h_0}{\partial x_1} & \text{in}\Omega \\ p_1 = 0 & \text{on } \partial\Omega \end{cases} \tag{6}$$

and p_2 is the solution of:

$$\begin{cases} \nabla \cdot [(a + h_0(x))^3 \nabla p_2] = -1 & \text{in } \Omega \\ p_2 = 0 & \text{on } \partial\Omega \end{cases} \tag{7}$$

The Lienard equation is commonly used in systems exhibiting nonlinear damping and restoring forces, making it suitable for modeling the behavior of lubricated contact surfaces. Using the classical notation $a_1(t) = a(t)$ and $a_2(t) = a'(t)$, the second-order differential equation (5) can be rewritten as a first-order system. This system is described by the following set of equations:

$$\begin{cases} a_1,(t) = a_2, \\ a_2,(t) = -g_2(a_1)a_2 + g_1(a_1) - F, \end{cases} \tag{8}$$

where $(a_1, a_2) \in U = \mathbb{R}_+^* \times \mathbb{R}$, with $\mathbb{R}_+^*$ indicating that $a_1(t)$ is strictly positive (since $a(t) > 0$) and $a_2(t) \in \mathbb{R}$. In this system: $a_1,(t) = a_2(t)$ represents the relationship between the displacement and its rate of change. The second equation describes the evolution of $a_2(t)$, which involves the terms $g_2(a_1)$, $g_1(a_1)$, and the external force F. The functions $g_2(a_1)$ and $g_1(a_1)$ are derived from the specific form of the problem, potentially corresponding to nonlinear damping and restoring forces that govern the displacement. This system now

describes the dynamics of $a(t)$ and its rate of change in terms of two first-order differential equations. The verified initial conditions are given by:

$$\begin{cases} a_1(0) = a_1^0 \\ a_2(0) = a_2^0 \end{cases} \tag{9}$$

2.1 *Some preliminaries and a local existence result*

Let's start by studying the properties of g_1 and g_2 in order to extract the maximum amount of information about the system (8)-(9).

Proposition 1: The functions g_1 and g_2 are of class C^∞, strictly positive, and satisfy the following conditions:

$$\lim_{a\to\infty} g_i(a) = 0 \quad i = 1,2. \tag{10}$$

with the convergence order:

$$|g_i(a)| \leq \frac{C}{a^3} \quad i = 1,2 \quad \forall a > 0 \quad \text{with } C > 0 \tag{11}$$

Proof: The positivity of g_1 and g_2 follows from the maximum principle. The regularity C^∞ is proven as in Proposition 3.2.1 of [15], and their convergence to 0 is established in Proposition 3.2.2 of [5].

Proposition 1 provides the classical result as in [14] with hte following Theorem:

Theorem 1: *For any $(a_1^0, a_2^0) \in U$, there exists a solution of the system (8) - (9) with local uniqueness in time, and the solution belongs to $C^\infty \times C^\infty$.*

2.2 *Global existence in time*

In this section, we will provide conditions for the existence or global non-existence of the solution to the problem (8) - (9). Let $T_{\max}$ denote the maximal existence time of the solution to this problem. We will demonstrate that the global existence or non-existence of a solution depends on the behavior of the functions $g_1(a_1)$ and $g_2(a_1)$ as a_1 tends to 0.

2.3 *Sufficient conditions of global existence*

Let's introduce the functional:

$$V: U \to \mathbb{R}$$
$$V(a) = V(a_1, a_2) = \frac{1}{2}a_2^2 - G_1(a_1) + Fa_1$$

with: $G_1(a_1) = \int_1^{a_1} g_1(s)ds$ We have the following result:

Proposition 2: If $(a_1(t), a_2(t))$ is a solution of (8), then the function: $t \to V(a_1(t), a_2(t))$ is decreasing.

Proof: We have:

$$\begin{aligned}\frac{\mathrm{d}}{\mathrm{dt}}V(a_1(t),a_2(t)) &= \frac{\partial V}{a_1}{a_1}' + \frac{\partial V}{a_2}{a_2}' \\ &= [-g_1(a_1)+F]a_2 + a_2[-g_2(a_1)a_2 + g_1(a_1) - F] \\ &= -a_2^2 g_2(a_1)\end{aligned}$$

Since $g_2(a_1) > 0$, we obtain the result.

Proposition 3: let us suppose $T_{max} < \infty$. Then, there exists an increasing sequence $t_n \to T_{max}$ with $t_0 = 0$ such that:

$$a_1(t_n) \to 0.$$

Proof: Let t_n be an increasing sequence that tends to $T_{\max}$ (for example, $t_n = T_{\max}\left(1 - \frac{1}{n}\right)$ if $n \geq 1$ and $t_0 = 0$). Then, from Proposition 2, the sequence $V(a_1(t_n), a_2(t_n))$ is decreasing. Hence, we have the inequality:

$$\tfrac{1}{2}[a_2(t_n)]^2 + Fa_1(t_n) \leq \tfrac{1}{2}(a_2^0)^2 + Fa_1^0 - G_1(a_1^0) + G_1(a_1(t_n)),\ \forall n \in \mathbb{N}. \quad (12)$$

On the other hand, from Proposition 1, we know that:

$$G_1(a) \leq \int_1^\infty g_1(s)\,ds < \infty, \quad \forall a > 0.$$

This implies, from equation (10), that the sequences $a_1(t_n)$ and $a_2(t_n)$ are bounded. Thus, there exists a subsequence of t_n, again denoted t_n, and constants $\hat{a}_1 \geq 0$ and $\hat{a}_2 \in \mathbb{R}$ such that:

$$a_1(t_n) \to \hat{a}_1 \quad \text{and} \quad a_2(t_n) \to \hat{a}_2 \quad \text{as} \quad n \to \infty. \quad (13)$$

It is well known (see [1]) that $(\hat{a}_1, \hat{a}_2)$ necessarily belongs to the boundary of the domain $]0,\infty[\times\mathbb{R}$, which implies that $\hat{a}_1 = 0$. This concludes the proof.

We can state the following global existence result:

Proposition 4: If $\frac{1}{2}(a_2^0)^2 - \int_0^{a_1^0} g_1 + Fa_1^0 < 0$, then $T_{max} = +\infty$

Proof: Suppose that $T_{\max} < \infty$. Let ι_n be the sequence defined in Proposition 3. Then we have the following inequality:

$$\tfrac{1}{2}[a_2(t_n)]^2 - G_1(a_1(t_n)) + Fa_1(t_n) \leq \tfrac{1}{2}(a_2^0)^2 + Fa_1^0 - G_1(a_1^0). \quad (9)$$

Taking the limit as $n \to \infty$, we obtain:

$$0 \leq \tfrac{1}{2}(a_2^0)^2 - [G_1(a_1^0) - G_1(0)] + Fa_1^0, \quad (14)$$

where $G_1(0)$ can either be a finite value or equal to ∞. By assumption, this leads to a contradiction. Hence, the result follows.

Corollary 2.1: *If $\int_0^1 g_1(s)\,ds = \infty$, then we have global existence in time for all $a_1^0 > 0$, $a_2^0 \in \mathbb{R}$, and $F > 0$.*

If $\int_0^1 g_1(s)\,ds < \infty$, then global existence in time is guaranteed provided that the initial data is "small" in the following sense:

$$\frac{1}{2}(a_2^0)^2 + Fa_1^0 < \int_0^{a_1^0} g_1(s)\, ds.$$

We now provide conditions on h_0 to ensure global existence in time for both the case of line contact and point contact.

Line Contact: For the case of line contact, the gap function $h_0(x)$ typically depends on the horizontal coordinate x, but remains constant along the contact width. In this case, the function $h_0(x)$ must satisfy the following condition to ensure global existence in time:

$$\int_0^{h_0(x)} g_1(s)ds \text{ is finite and sufficiently large for all } x.$$

This condition ensures that the integral of $g_1(s)$ does not cause the solution to blow up in finite time, and it guarantees that the evolution of the pressure and displacement remains stable.

Point Contact: In the case of point contact, $h_0(x)$ is typically a constant (representing a point contact between two surfaces). The global existence in time for point contact requires that the function h_0 is such that:

$$h_0 > 0 \quad \text{and} \quad \int_0^{h_0} g_1(s)ds \text{ is large enough to avoid singularities.}$$

This ensures that the lubricant film does not collapse or cause unbounded pressure under the applied force F, thus leading to a globally stable system.

In both cases, the key factor for global existence is the appropriate choice of h_0 such that the conditions on the functions $g_1(s)$ hold, ensuring that the system behaves well over time without the solution blowing up.

Theorem 2: *Suppose that besides* (H_1), h_0 *verifies the hypothesis:*

$$\begin{cases} \text{There exists } h_1 \in C^1(\bar{\Omega}) \text{ such that } h_1 > 0 \text{ and} \\ h_0(x) = (-x_1)^\alpha h_1(x) \quad \text{(line contact)} \end{cases} \qquad (H_1)$$

If $\alpha \geq 2$*, then there is global existence in time of a solution of (8) - (9) in* $C^\infty(\mathbb{R}^+) \times C^\infty(\mathbb{R}^+)$ *for all* $a_1^0 > 0$, $a_2^0 \in \mathbb{R}$, *and* $F > 0$.

Proof: It is evident that $\int_0^1 g_1(s)\, \mathrm{d}s = +\infty$ when $\alpha \geq 2$ (Theorem 2.3.2 in [15]). Consequently, as a result of Corollary 2.1, we obtain the desired conclusion.

Following the same reasoning as in the previous proposition, we demonstrate:

Theorem 3: *Suppose that besides* (H_1), h_0 *verifies the hypothesis:*

$$\begin{cases} \text{There exists } h_1 \in C^1(\bar{\Omega}) \text{ such that } h_1 > 0 \text{ and} \\ h_0(x) = |x|^\alpha h_1(x) \quad \text{(punctual contact)} \end{cases} \qquad (H_2')$$

If $\alpha \geq 3$*, then there is global existence in time of a solution of (8) - (9) in* $C^\infty(\mathbb{R}^+) \times C^\infty(\mathbb{R}^+)$ *for all* $a_1^0 > 0$, $a_2^0 \in \mathbb{R}$, *and* $F > 0$.

2.4 *Sufficient conditions of global non-existence*

In the following, we study the conditions under which $T_{\max} < \infty$, that is, the possibility for the distance between the two rigid surfaces to become equal to zero in finite time (Proposition 3). We start with the following technical result:

Lemma 1: *Let I be a time interval of the form $]0,T[$ with $T > 0$ such that $a_2(t) < 0 \ \ \forall t \in I$. Then $\forall \beta > 0$ and $\forall t \in I$, we have:*

$$a_2^2(t) \geq e^{\beta a_1}\left[(a_2^0)^2 e^{-\beta a_1^0} + \int_{a_1(f)}^{a_1^0}\left[-\frac{1}{\beta}g_2^2(s) - 2g_1(s) + 2F\right]e^{-\beta s}\,ds\right] \quad (15)$$

Proof: Since $a_1'(t) = a_2(t) < 0$, the function $t \in [0,T[\mapsto a_1(t) \in [a_1(T), a_1^0]$ is bijective. This allows us to express a_2 as a function of a_1, and we can write the following differential equation:

$$\frac{da_2}{da_1} = \frac{-a_2 g_2(a_1) + g_1(a_1) - F}{a_2} \quad (16)$$

which simplifies to:

$$a_2 \frac{da_2}{da_1} = -a_2 g_2(a_1) + g_1(a_1) - F \quad (17)$$

Next, we apply the following inequality, which holds for all $\beta > 0$:

$$-2a_2 g_2(a_1) \leq \beta a_2^2 + \frac{1}{\beta}g_2^2(a_1) \quad (18)$$

This inequality helps us obtain a bound on the derivative of

$$\frac{d}{da_1}[a_2^2] \leq \beta a_2^2 + \frac{1}{\beta}g_2^2(a_1) + 2[g_1(a_1) - F] \quad (19)$$

Now, we consider the function $a_2^2 e^{-\beta a_1}$, and differentiate it with respect to a_1. Using the chain rule, we obtain:

$$\frac{d}{da_1}\left[a_2^2 e^{-\beta a_1}\right] = e^{-\beta a_1}\frac{d}{da_1}[a_2^2] - \beta a_2^2 e^{-\beta a_1} \quad (20)$$

By applying the inequality (19) into this, we get the following bound:

$$\frac{d}{da_1}\left[a_2^2 e^{-\beta a_1}\right] \leq e^{-\beta a_1}\left[\frac{1}{\beta}g_2^2(a_1) + 2[g_1(a_1) - F]\right]e^{-\beta a_1} \quad (21)$$

To complete the proof, we integrate both sides of the inequality between a_1 and a_1^0. The left-hand side is the to (a_2). By substituting it into the equation for $\frac{d}{da_1}[a_2^2]$, we get the following estimate:

Proof: The derivative of $a_2^2 e^{-\beta a_1}$, and the right-hand side is an integral of terms that are bounded by the functions $g_1(a_1)$ and $g_2(a_1)$, along with the constant force F. After performing the integration, we can establish bounds on the solution $a_2(t)$ as a function of time.

Proposition 5: Let $a_2^0 < 0$ and suppose that the following condition holds: there exists $\beta_0 > 0$ such that

$$(a_2^0)^2 e^{-\beta_0 a_1} > \int_0^{a_1^0} \left[\frac{1}{\beta_0}(g_2(s))^2 + 2(g_1(s) - F)\right] e^{-\beta_0 s}\, ds, \quad \forall a_1 \in [0, a_1^0] \tag{22}$$

Then, we have $T_{\max} < \infty$.

Proof: Assume that $T_{\max} = \infty$, i.e., the solution exists for all time. We will derive a contradiction by analyzing the behavior of the system. Let L be defined as:

$$L = \inf_{b \in [0, a_1^0]} \left\{(a_2^0)^2 e^{-\beta_0 a_1^0} - \int_0^{a_1^0} \left[\frac{1}{\beta_0}(g_2(s))^2 + 2(g_1(s) - F)\right] e^{-\beta_0 s}\, ds\right\} \tag{23}$$

By assumption, $L > 0$. Since $a_2^0 < 0$, there exists a time interval $I_1 = [0, T_1]$ such that for all $t \in I_1$, we have $a_2(t) < 0$, and consequently, for all $t \in I_1$,

$$a_1(t) < a_1^0. \tag{24}$$

Assume that $T_1 = \infty$. If T_1 were finite, then we would have $a_2(T_1) = 0$, which contradicts the assumptions and the positivity of L. Since $T_1 = \infty$, we now know that for all $t \geq 0$,

$$a_2(t) \leq -\sqrt{L}. \tag{25}$$

Thus, the displacement $a_1(t)$ satisfies:

$$a_1(t) = a_1^0 + \int_0^t a_2(s)\, ds \leq a_1^0 - \sqrt{L}t \quad \forall t \geq 0. \tag{26}$$

For sufficiently large t, $a_1(t)$ will become negative, contradicting the condition that $a_1(t) > 0$. This contradiction implies that our assumption that $T_{\max} = \infty$ must be false. Hence, we conclude that $T_{\max} < \infty$.

Remark 1:

- The hypothesis of Proposition 5 is verified in at least the following two situations:
- If g_1 and g_2 are such that:

  $$\int_0^1 g_2^2(s)\, \mathrm{d}s < \infty \quad \text{and} \quad \int_0^1 g_1(s)\, \mathrm{d}s < \infty,$$

  then for all $a_1^0 > 0$ and $F > 0$, there exists $a_2^0 < 0$ with $|a_2^0|$ sufficiently large such that (22) is satisfied.
- If g_1 and g_2 are bounded on $]0, \infty[$, then a sufficient condition to have (22) is:

  $$F > \sup_{s \in [0, a_1^n]} g_1(s),$$

  because by taking β_0 large enough, the right-hand side of (22) becomes negative.

Theorem 4: *Suppose that* h_0 *satisfies the hypothesis* (H_1) *and the hypothesis* (H_2) *with* $\alpha \in]0,1[$. *Then for all* $a_1^0 > 0$ *and* $a_2^0 < 0$, *and for all* $F > sup_{s\in]0,a_1^q]} g_1(s)$, *we have:*

$$T_{\max} < +\infty. \tag{27}$$

Proof: Since h_0 verifies (H_2) with $0 < \alpha < 1$, Theorem 2.3.1 [15] implies that g_1 is bounded on $[0, \infty]$. The application:

$$\varphi \in H_0^1(\Omega, h_0, h_0^3) \to \int_\Omega x_1 \frac{\partial \varphi}{\partial x_1} \, \mathrm{dx} \in \mathbb{R}$$

is linear and continuous because:

$$\int_\Omega |x_1| \left|\frac{\partial \varphi}{\partial x_1}\right| \leq \left[\int_\Omega \frac{(x_1)^2}{h_0^3} \, \mathrm{dx}\right]^{1/2} \left[\int_\Omega h_0^3 \frac{\partial \varphi}{\partial x_1} \, \mathrm{dx}\right]^{1/2}$$

Since $\alpha < 1$, we have $\int_\Omega \frac{(x_1)^2}{h_0^3} \, \mathrm{dx} < \infty$. We can then, as in Theorem 2.3.1 [15], deduce that g_2 remains bounded on $]0, +\infty[$ for $0 < \alpha < 1$. By applying Remark 1 and Proposition 5, we find the sought result.

Following the same reasoning as in the previous proposition, we show:

Theorem 5: *Suppose that* h_0 *satisfies the hypothesis* (H_1) *and the hypothesis* (H_2') *with* $\alpha \in]0, \frac{3}{2}[$. *Then for all* $a_1^0 > 0$ *and* $a_2^0 < 0$, *and for all* $F > sup_{s\in[0,a_1^n]} g_1(s)$, *we have*

$$T_{\max} < +\infty$$

2.5 *Balance points and stability*

It is obvious that $a^* = (a_1^*, a_2^*)$ is a stationary point of problem (8) if and only if:

$$\begin{cases} a_2^* = 0 \\ g_1(a_1^*) = F \end{cases}$$

We have the following result:

Proposition 6: Under the assumption:

$$\lim_{a\to 0} g_1(a) > F,$$

there exists at least one stationary point of (8). Moreover, if g_1 is differentiable and $g_1'(s) < 0$ for all $s > 0$, then this point is unique and asymptotically stable.

Proof: The existence is an immediate consequence of Proposition 1 and the uniqueness is elementary. For stability, we compute the eigenvalues of the Jacobian matrix at a^* of the right-hand side of (8):

$$A = \begin{pmatrix} 0 & 1 \\ g_1'(a_1^*) & -g_2(a_1^*) \end{pmatrix} \tag{28}$$

The eigenvalues are the roots of the equation:

$$\lambda^2 + g_2(a_1^*)\lambda - g_1'(a_1^*) = 0 \tag{29}$$

Since $g_{1'}(a_1^*) < 0$ and $g_2(a_1^*) > 0$, it is evident that the real parts of the eigenvalues are strictly negative, which, according to classical theory, leads us to the desired conclusion.

Now, suppose that h_0 satisfies the conditions (H_1) and (H_2). The results in [15] guarantee that a stationary solution exists for all $F > 0$ if $\alpha \geq 1$, or for F not exceeding $\int_\Omega p_0 \, \mathrm{dx}$ if $\alpha < 1$, where p_0 is the solution of (P_{01}). Furthermore, if $\alpha = 1$ and h_1 is constant, it follows that the stationary solution is unique and asymptotically stable.

Remark 2: In one dimension, we have uniqueness and asymptotic stability under the assumptions $\alpha = 1$ and h_1 constant.

3. Asymptotic behavior in the Variational equation

In this section, for simplicity, we assume that $\Omega^+ = \{x \in \Omega : p(x,t) > 0\}$, and that h_0 is non-increasing. We now turn our attention to studying the asymptotic behavior of the solution p of the problem defined by equation (30). To formulate the limit problem, we first define the set $\mathcal{K}_{\delta_1}$, which is the closure of $\mathcal{K} = \{\varphi \in H_0^1(\Omega) : \varphi \geq 0\}$ with respect to the norm of $H_0^1(\Omega, h_0^{2\delta_1}, h_0^3)$. It is important to note that $\mathcal{K}_{\delta_1}$ is a closed convex set in $H_0^1(\Omega, h_0^{2\delta_1}, h_0^3)$.

We now introduce the limit problem:

$$\begin{cases} \text{Find } p_0 \in \mathcal{K}_{\delta_1} \text{such that} \\ a'' = \int_{\Omega^+} p \, dx - F \end{cases} \tag{30}$$

This leads us to the following equation:

$$\begin{cases} \int_{\Omega^+} (h_0 + a)^3 \nabla p \cdot \nabla \varphi \, dx = \int_{\Omega^+} h_0 \frac{\partial \varphi}{\partial x_1} + a' \varphi \, dx, \quad \forall \varphi \in \mathcal{K}_{\delta_1}, \\ a'' = \int_{\Omega^+} p \, dx - F \end{cases} \tag{31}$$

We proceed by deriving existence, uniqueness, and convergence results for this problem. By exploiting linearity, we can express the problem (31) as a second-order ordinary differential equation (ODE) of the form of a Lienard equation:

$$\begin{cases} a''(t) = -g_2(a(t))a'(t) + g_1(a(t)) - F \\ a(0) = a_1^0, \quad t = 0 \\ a'(0) = a_2^0 \end{cases} \tag{32}$$

In this formulation, the functions $g_i(a)$ for $i = 1,2$ are defined as:

$$g_i(a) = \int_{\Omega^+} p_i(x) dx, \quad \text{for all } a > 0, \tag{33}$$

where p_1 and p_2 are solutions to the following boundary value problems: For p_1:

$$\begin{cases} \nabla \cdot [(a + h_0(x))^3 \nabla p_1] = h_0 & \text{in } \Omega^+, \\ p_1 = 0 & \text{on } \partial\Omega^+, \end{cases} \tag{34}$$

and for p_2:

$$\begin{cases} \nabla \cdot [(a + h_0(x))^3 \nabla p_2] = -1 & \text{in } \Omega^+, \\ p_2 = 0 & \text{on } \partial\Omega^+. \end{cases} \tag{35}$$

Next, using the classical notation $a_1(t) = a(t)$ and $a_2(t) = a'(t)$, equation (32) can be reformulated as a first-order differential system:

$$\begin{cases} a_1'(t) = a_2, \\ a_2'(t) = -g_2(a_1)a_2 + g_1(a_1) - F, \\ a_1(0) = a_1^0, \\ a_2(0) = a_2^0 \end{cases} \tag{36}$$

In this form, we are looking for a solution (a_1, a_2) in the set $U = \mathbb{R}_+^* \times \mathbb{R}$ that satisfies the system of equations described above.

The next steps in the analysis involve examining the properties of the solutions to this system, including existence, uniqueness, and asymptotic behavior, which can be derived using standard techniques in the theory of ordinary differential equations, specifically focusing on the stability and the behavior of the solution as $t \to \infty$.

4. Discretization and results

In this section, we present the numerical simulation of the Reynolds equation (3) introduced in this work. The objective of the simulation is to solve both the one-dimensional and two-dimensional PDEs that involve nonlinear behavior. Additionally, we discuss the choices made in discretization, time-stepping methods, boundary conditions, and provide a detailed analysis of the computational results. The model we aim to solve is given by the following PDE:

$$\int_\Omega (h_0 + a)^3 \nabla p \cdot \nabla \phi = \int_\Omega h_0 \frac{\partial \phi}{\partial x_1} + a' \phi, \quad \forall \phi \in K_{\delta_1} \tag{37}$$

and the equation for a'' is:

$$a'' = \int_\Omega p \, dx - F. \tag{38}$$

Here, p is the variable in the domain Ω, h_0 and a are constants, ϕ represents the solution to the PDE, and a' and F are additional parameters, K_{δ_1} is the Sobolev space $K_{\delta_1} = H_0^1(\Omega)$. The goal is to solve for ϕ, which models some physical or geometrical property in the system. To derive the full discretization of the given equations using the Finite Volume Method (FVM) [22, 23, 24]. We first need to understand the structure of the equations and how they can be discretized in space. Below, we walk through each step, explaining the finite volume discretization and how it applies to the given system of equations. The first equation is a weak form of a PDE, which involves the unknown field ϕ and pressure p. We aim to solve it over a domain Ω.

$$\int_\Omega (h_0 + a)^3 \nabla p \cdot \nabla \phi \, dx = \int_\Omega h_0 \frac{\partial \phi}{\partial x_1} \, dx + \int_\Omega a' \phi \, dx, \quad \forall \phi \in K_{\delta_1} \tag{39}$$

The second equation provides the relationship for a'':

$$a'' = \int_\Omega p \, dx - F. \tag{40}$$

The Finite Volume Method is commonly used for conservation laws and involves discretizing the domain into control volumes and integrating the governing equations over each volume. Let us discretize each part of the system, assuming that the domain Ω is divided into N control volumes indexed by i. Each control volume corresponds to a grid cell in the spatial mesh. We start with the weak form:

$$\int_\Omega (h_0 + a)^3 \nabla p \cdot \nabla \phi \, dx = \int_\Omega h_0 \frac{\partial \phi}{\partial x_1} \, dx + \int_\Omega a' \phi \, dx. \tag{41}$$

The left-hand side involves a term with gradients of p and ϕ. In the finite volume method, we discretize the gradient of the fields using their values at cell centers or boundaries.

We approximate the gradient terms ∇p and $\nabla \phi$ using finite differences between neighboring control volumes. Let p_i and ϕ_i represent the values of pressure and the field ϕ at the i-th control volume. For the gradient of p, the finite volume approximation is given by:

$$\nabla p \approx \frac{p_{i+1} - p_i}{\Delta x}, \tag{42}$$

where Δx is the size of the control volume. We can similarly approximate $\nabla \phi$ as:

$$\nabla \phi \approx \frac{\phi_{i+1} - \phi_i}{\Delta x}.$$

Therefore, the term $\nabla p \cdot \nabla \phi$ can be approximated as:

$$\nabla p \cdot \nabla \phi \approx \frac{(p_{i+1} - p_i)(\phi_{i+1} - \phi_i)}{(\Delta x)^2}.$$

The term $(h_0 + a)^3$ is evaluated at the cell center, so the integral for each control volume becomes:

$$\int_{V_i} (h_0 + a)^3 \nabla p \cdot \nabla \phi \, dx \approx (h_0 + a_i)^3 \frac{(p_{i+1} - p_i)(\phi_{i+1} - \phi_i)}{(\Delta x)^2}.$$

The right-hand side consists of two terms:

- The first term involves $h_0 \frac{\partial \phi}{\partial x_1}$. Using a central difference scheme, this becomes:

$$h_0 \frac{\partial \phi}{\partial x_1} \approx h_0 \frac{\phi_{i+1} - \phi_i}{\Delta x}.$$

- The second term is $a' \phi$, which is evaluated at the cell center:

$$\int_{V_i} a' \phi \, dx \approx a'_i \phi_i \Delta x$$

Now, we can combine all terms to get the finite volume discretization of the first equation:

$$(h_0 + a_i)^3 \frac{(p_{i+1} - p_i)(\phi_{i+1} - \phi_i)}{(\Delta x)^2} = h_0 \frac{\phi_{i+1} - \phi_i}{\Delta x} + a'_i \phi_i \Delta x. \tag{43}$$

This equation relates the pressure p and the field ϕ at neighboring control volumes. The equation for a'' is given as:

$$a'' = \int_{\Omega} p\, dx - F.$$

In finite volume, we approximate the integral of p over the control volumes:

$$\int_{V_i} p\, dx \approx p_i \Delta x.$$

Thus, the equation for a'' in discrete form is:

$$a''_i = \sum_{i=1}^{N} p_i \Delta x - F$$

where p_i is the pressure at the i-th control volume, and F is some constant or known value. Summarizing the discretized system, we have two key equations:

$$\begin{cases} (h_0 + a_i)^3 \frac{(p_{i+1} - p_i)(\phi_{i+1} - \phi_i)}{(\Delta x)^2} = h_0 \frac{\phi_{i+1} - \phi_i}{\Delta x} + a'_i \phi_i \Delta x, \\ a''_i = \sum_{i=1}^{N} p_i \Delta x - F. \end{cases}$$

The discretization assumes periodic or Dirichlet boundary conditions for the fields p and ϕ. For Dirichlet boundary conditions, we set the values of p and ϕ at the boundaries to known values (e.g., $p = 0$ or $\phi = 0$). The finite volume method naturally ensures conservation of the quantities being solved for, as the fluxes across control volumes are balanced. The system is nonlinear due to the $(h_0 + a)^3$ term, which require an iterative solution technique using Newton's method to solve for ϕ and p. Finally, the main resolution procedure of the studied problem is summarized in Algorithm 1.

Algorithm 1 Finite Volume Method for Steady-State Reaction-Diffusion Equation with Pressure Correction

Input: Parameters L, Nx, function $a(x)$, true solution $\phi_{\text{true}}(x)$. Define control volumes x_i for $i = 1,2, \ldots, N$ and cell spacing $\Delta x = L/Nx$. Define the reaction term $R(x) = -0.1\phi_{\text{true}}(x)$. Define derivatives: $a'(x) = \frac{d}{dx}a(x)$. Set initial guess for $\phi = 0$ and $p = 1$. max_iter, tolerance, under-relaxation factor α_r, under-relaxation factor for pressure α_p

for iter $= 1$ to max_iter **do**

Store old values: $\phi_{\text{old}} \leftarrow \phi$, $p_{\text{old}} \leftarrow p$

Compute Fluxes

for each control volume $i = 1$ to N **do**

Compute flux at interfaces $i + 1/2$ and $i - 1/2$:

$$\text{Flux}_{i+1/2} = -\frac{\phi_{i+1} - \phi_i}{\Delta x}, \quad \text{Flux}_{i-1/2} = -\frac{\phi_i - \phi_{i-1}}{\Delta x}$$

end for

Assemble Coefficients for phi

for each control volume $i = 1$ to N **do**

Compute coefficients:

- $a_w = \frac{1}{\Delta x}$, $a_e = \frac{1}{\Delta x}$, $a_p = a_w + a_e$

end for

Discretized phi Equation

Assemble the sparse matrix $\mathbf{A}_\phi$ representing the discretized spatial operator

Solve Linear System for phi

$$\phi = \mathbf{A}_\phi^{-1}\mathbf{b}_\phi$$

Calculate Gradient of Pressure

for each control volume $i = 1$ to N **do**

Calculate the gradient of pressure at each face:

$$\text{grad\_p}_{i+1/2} = \frac{p_{i+1}-p_i}{\Delta x}, \quad \text{grad\_p}_{i-1/2} = \frac{p_i-p_{i-1}}{\Delta x}$$

end for

Solve Linear System for pressure correction

$$p' = \mathbf{A}_p^{-1}\mathbf{b}_p$$

Update Pressure

$$p = p + \alpha_p p'$$

Apply under-relaxation to phi

$$\phi = \alpha_r \phi + (1-\alpha_r)\phi_{\text{old}}$$

end for

Output: Steady-state solution ϕ, pressure p, and relative error.

4.1 *One dimensional Equation*

For the numerical realization, we start by a one-dimentional test. The domain $[0, L]$ is divided into Nx control volumes of size $\Delta x = L/Nx$. Fluxes are approximated using a central difference scheme. A SIMPLE-like algorithm is implemented for pressure correction [24, 25]. Under-relaxation factors $\alpha_r = 0.1$ (for ϕ) and $\alpha_p = 0.1$ (for p) are used for stable convergence. The discrete spatial operator is encoded as a sparse matrix for efficient solution. The linear system is solved using direct matrix inversion. We consider a one-dimensional reaction-diffusion equation of the form:

$$\nabla \cdot ((a(x) + h_0(x))^3 \nabla p) = R(x), \tag{45}$$

where ϕ is the field variable, p is the pressure, and $a(x)$ is a spatially varying coefficient. The term $R(\phi)$ represents a reaction term, which could be nonlinear. For simplicity, we choose a linear reaction term of the form:

$$R(x) = -0.1\phi_{\text{true}}(x),$$

with

$$\phi_{true}(x) = \exp(-((x - L/2)^2)/0.1),$$

which is a Gaussian function centered at $x = L/2$, where L is the domain size.

The pressure term involves the gradient of the pressure $p(x)$, and ∇p represents the derivative of pressure with respect to space. The spatially varying coefficient $a(x)$ is chosen as:

$$a(x) = \sin(x).$$

The goal is to numerically solve this equation using a finite difference method and update both the field variable ϕ and pressure p at each time step.

- Domain Length: $L = 10$
- Control Volumes: $Nx = 100$
- Cell Size: $\Delta x = L/Nx$
- Under-relaxation: $\alpha_r = 0.1$, $\alpha_p = 0.1$
- Convergence Tolerance: 10^{-6}
- True Solution: Gaussian distribution $\phi_{\text{true}}(x) = \exp(-((x - L/2)^2)/0.1)$
- Boundary conditions: Homogeneous Dirichlet Boundary Conditions.

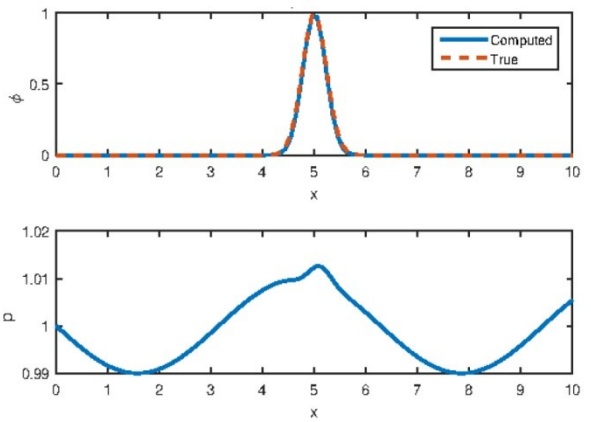

Figure 2

The computed ϕ compared to the true one ϕ_{true} and also the final pressure p.

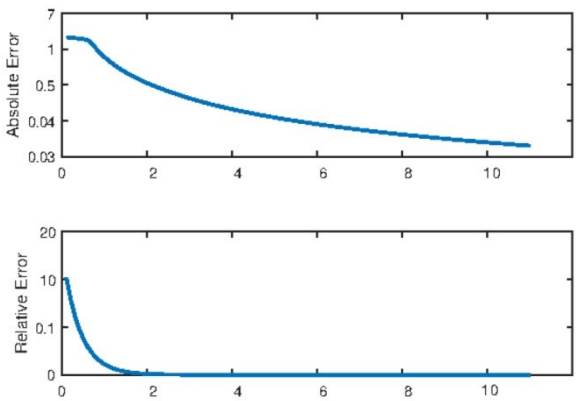

Figure 3

The evolution of the absolute and relative errors.

The numerical method provides a steady-state solution for $\phi(x)$ in Figure 2, and the pressure $p(x)$. Solution profiles are plotted for analysis, and the relative error is computed by using the true solution in Figure 3. This example successfully simulates a steady-state reaction-diffusion equation with spatial variation using FVM. The method demonstrates good stability, and allows a robust steady-state solution to be obtained for the problem.

4.2 *Two dimensional Equation*

The computational domain is a two-dimensional square grid with dimensions $L_x = L_y = 1$, discretized into $Nx = 50$ and $Ny = 50$ grid points in the x_1 and x_2 directions. The grid spacing in each direction is calculated as:

$$\Delta x = \frac{L_x}{N_x - 1}, \quad \Delta y = \frac{L_y}{N_y - 1}.$$

This results in a uniform grid over the domain, and the computational points are generated using the `meshgrid` function in MATLAB. For this simulation, the following parameter values were chosen:

- $h_0 = 1$, which is a constant that governs the strength of the diffusion process.
- $a = 0.5$, which is another constant that affects the nonlinear diffusion term.
- $a' = 1$, which is a constant that appears in the reaction term of the equation.
- $F = 0.1$, a constant that represents an external forcing term.
- p is taken as a uniform grid of ones for simplicity.

These values are typical for numerical testing and are chosen to represent a general scenario where the diffusion and reaction processes are nontrivial but not excessively large, ensuring that the simulation runs efficiently. The initial guess for the solution ϕ is chosen as a sinusoidal function:

$$\phi(x_1, x_2) = \sin(\pi x_1)\sin(\pi x_2).$$

This choice is made to provide a smooth initial solution that can be easily compared with analytical solutions. The true solution for comparison is also based on this form, as it simplifies the error calculation and provides a clear test case. We apply Dirichlet boundary conditions to all four edges of the domain, i.e., we set $\phi = 0$ on the boundaries of the computational domain. This is a common choice for such problems and is appropriate when the solution is expected to decay to zero at the edges of the domain or when there is no flux across the boundaries. The recovered solution ϕ is depicted in Figure 4, where comparison with the original solution is done and also the relative error. This study successfully simulates a steady-state reaction-diffusion equation with spatial variation using FVM when a is constant. The method demonstrates good stability, and allows a robust steady-state solution to be obtained for the problem.

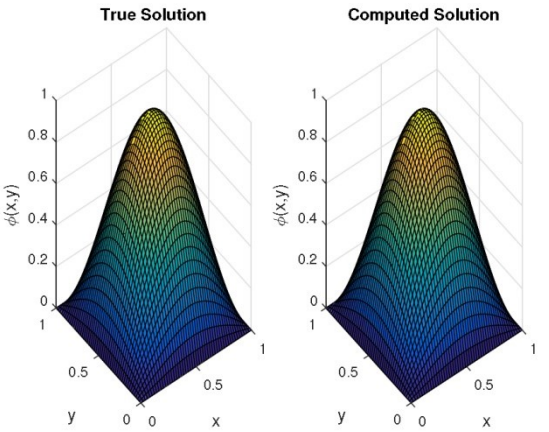

(a) Restored ϕ and the true one

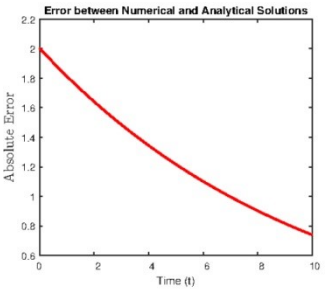

(b) The evolution of the absolute error

Figure 4

The evolution of the restored function ϕ and the associated absolute error.

After solving the PDE, the computed solution is compared with the true solution, $\phi_{\text{true}} = \sin(\pi x_1)\sin(\pi x_2)$. The error is calculated as the absolute difference between the computed solution and the true solution:

$$\text{Error}(x_1, x_2) = |\phi_{\text{computed}}(x_1, x_2) - \phi_{\text{true}}(x_1, x_2)|.$$

This provides a quantitative measure of how well the numerical solution matches the true solution.

4.3 *The evolution equation*

We are solving the following reaction-diffusion equation with pressure correction:

$$\frac{\partial \phi}{\partial t} = \nabla \cdot ((h_0 + a(x))^3 \nabla \phi) + \left(h_0 \frac{\partial \phi}{\partial x_1} + a'(x)\phi\right), \tag{46}$$

where $\phi(x, t)$ is the field we are solving for, h_0 is a constant, and $a(x)$, $a'(x)$, and $a''(x)$ are spatially varying coefficients. The equation governs the evolution

of $\phi(x,t)$, with pressure correction terms involved. Additionally, we also solve for the pressure $p(x,t)$ via the equation:

$$a''(x) = \int_{\Omega} p(x)\,dx - F,$$

where F is a constant (source term), and $p(x,t)$ is updated based on the evolution of $\phi(x,t)$. For spatial discretization, we use a uniform grid with spacing Δx over the domain $\Omega = [0, L]$. Let $x_i = i\Delta x$ for $i = 1,2,\ldots,Nx$, where Nx is the total number of grid points. The Laplacian operator $\nabla^2\phi$ is approximated using the second-order central finite difference scheme as:

$$\nabla^2\phi(x) \approx \frac{\phi_{i+1}-2\phi_i+\phi_{i-1}}{(\Delta x)^2}. \tag{47}$$

This discretization approximates the spatial derivatives of ϕ at each grid point. To approximate the gradient of $p(x)$, we use the central difference method:

$$\frac{\partial p}{\partial x}(x) \approx \frac{p_{i+1}-p_{i-1}}{2\Delta x}. \tag{48}$$

This provides a discrete approximation of the gradient at each point in the domain.

The time evolution is handled using a simple explicit Euler method, which updates $\phi(x,t)$ and $p(x,t)$ at each time step $t_n = n\Delta t$ as follows:

$$\phi^{n+1} = \phi^n + \Delta t\left[\nabla\cdot((h_0 + a(x))^3\nabla\phi^n) + \left(h_0\frac{\partial\phi^n}{\partial x_1} + a'(x)\phi^n\right)\right], \tag{49}$$

where ϕ^n is the field at time t_n and Δt is the time step. The pressure field $p(x,t)$ is updated using the equation:

$$p^{n+1} = p^n + \Delta t[a'(x)\cdot\phi^n + a''(x)], \tag{50}$$

where p^n is the pressure at time step t_n. The pressure correction term is incorporated by solving the following pressure update equation at each time step:

$$p^{n+1}(x) = p^n(x) + \Delta t[a'(x)\cdot\phi^n(x) + a''(x)]. \tag{51}$$

Here, the pressure correction term depends on the field $\phi(x,t)$ and its derivatives. This update ensures that the pressure is adjusted based on the current state of the field. The domain Ω is assumed to have Dirichlet boundary conditions for both $\phi(x,t)$ and $p(x,t)$:

$$\phi(0,t) = \phi(L,t) = 0, \quad p(0,t) = p(L,t) = 0 \tag{52}$$

These boundary conditions ensure that both fields $\phi(x,t)$ and $p(x,t)$ remain fixed at the ends of the domain.

Algorithm 2 Numerical Solution of Reaction-Diffusion Equation with Pressure Correction

Input: Parameters L, Nx, dt, T, initial conditions for $\phi(x,0)$, $p(x,0)$

Initialize:

- Set the initial condition for $\phi(x,0)$ and $p(x,0)$
- Compute the discrete Laplacian $D2$ and other necessary operators

for each time step t_n from 1 to Nt **do**

Compute the Laplacian of ϕ: $\nabla^2\phi^n(x)$

Compute the gradient of pressure: $\nabla p^n(x)$

Compute the reaction term: $R(\phi^n(x))$

Update $\phi^{n+1}(x)$ using the discretized equation:

$$\phi_i^{n+1} = \phi_i^n + \Delta t \left[\frac{\phi_{i+1}^n - 2\phi_i^n + \phi_{i-1}^n}{(\Delta x)^2} + h_0 \frac{\phi_{i+1}^n - \phi_{i-1}^n}{2\Delta x} + (a(x_i) + 1)^3 \frac{p_{i+1}^n - p_{i-1}^n}{2\Delta x} + h_0 \frac{\partial \phi^n}{\partial x_1} + a'(x_i)\phi_i^n\right]$$

Update pressure $p^{n+1}(x)$ using the pressure correction formula:

$$p_i^{n+1} = p_i^n + \Delta t[a'(x_i) \cdot \phi_i^n + a''(x_i)]$$

Apply boundary conditions:

$$\phi(0,t) = \phi(L,t) = 0, \quad p(0,t) = p(L,t) = 0$$

end for

Termination:

- The algorithm terminates after Nt time steps, or when a stopping criterion (e.g., steady-state solution) is met.

Output: Final solution for ϕ and p

We discretize the spatial derivatives using finite differences. The domain is discretized into a grid with Nx and Ny grid points in the x- and y-directions. The spatial step sizes are denoted by $\Delta x = h_x$ and $\Delta y = h_y$, where:

$$h_x = \frac{1}{Nx-1}, \quad h_y = \frac{1}{Ny-1}.$$

The grid points are stored in arrays X and Y, which represent the spatial coordinates. The PDE involves computing the gradient of ϕ, as well as the first and second derivatives of the function $a(x,y)$. For this, we use central differences to approximate the spatial derivatives:

$$\frac{\partial \phi}{\partial x} \approx \frac{\phi(x+1,y) - \phi(x-1,y)}{2h_x}, \quad \frac{\partial^2 \phi}{\partial x^2} \approx \frac{\phi(x+1,y) - 2\phi(x,y) + \phi(x-1,y)}{h_x^2},$$

Choice of Functions

For the spatially-varying function $a(x,y)$, we choose the following:

$$a(x,y) = \sin\big(\pi(x+y)\big).$$

The derivative of this function is:

$$a'(x,y) = \pi\cos\big(\pi(x+y)\big).$$

The second derivative of this function is:

$$a''(x,y) = -\pi^2\sin\big(\pi(x+y)\big).$$

We choose the constant $h_0 = 1$, which simplifies the equation and provides a baseline for comparison with more complex choices. For the function $p(x,y)$, we choose a simple constant function:

$$p(x,y) = 1.$$

The constant F is chosen as $F = 0$, which simplifies the second equation for a''. The results of the simulation are shown in Figure 5, where the evolution of $\phi(x, y)$ is plotted at different time steps. The relative error between the computed and true solutions is visualized in Figure 6. For different time steps, we observe that the computed solution closely matches the true solution after a sufficient number of iterations. The error decreases as the time step decreases, with the backward Euler method ensuring stability for larger time steps.

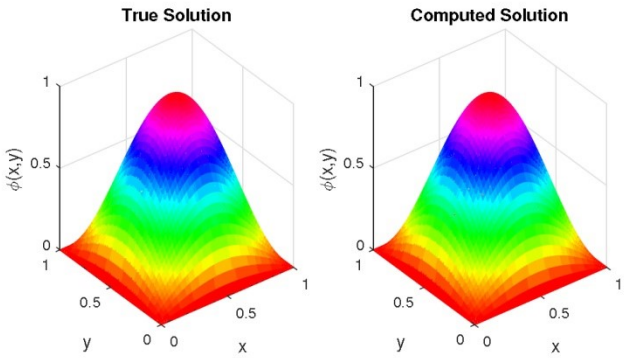

Figure 5
The computed and true $\phi(x, y)$.

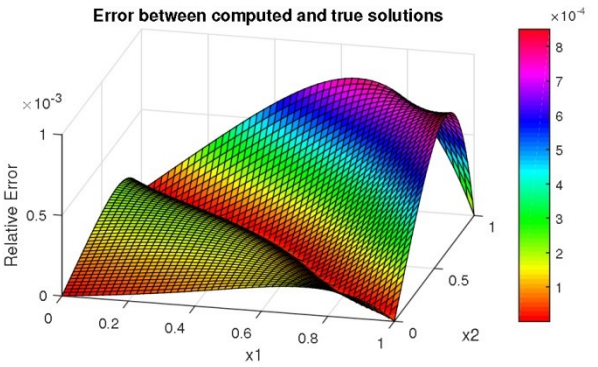

Figure 6
The evolution of the relative error.

We change now the function $a(x, y)$ to

$$a(x, y) = \sin\left(\pi^2(x + y)\right).$$

The numerical solution at final time step is plotted in Figure 7, showing the evolution of ϕ over time. We also show the final computed solution and compare it to the true solution. The error between the computed and true solutions is displayed as a surface plot, the L2 relative norm error and the L2

error norm are calculated to provide a measure of the overall accuracy. The results demonstrate that the computed solution converges to the true solution as the time progresses, although some discrepancies remain due to numerical errors inherent in the finite volume method. The absolute L2 error norm is around 10^{-4}, indicating that the solution is improving with each time step.

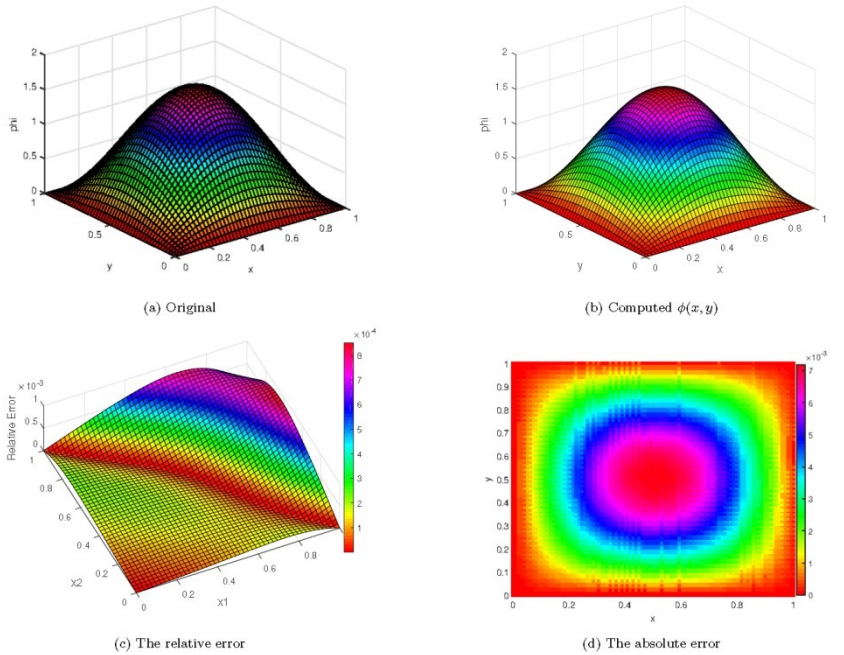

(a) Original (b) Computed $\phi(x, y)$

(c) The relative error (d) The absolute error

Figure 7

The numerical realization and the absolute and the relative error for the case when $\boldsymbol{a(x,y) = \sin(\pi^2(x+y))}$.

5. Real Applications

5.1 *Contaminant transport and biodegradation*

This application presents a time-dependent simulation of contaminant transport and biodegradation in a one-dimensional soil column. We model the transport of a contaminant (e.g., a volatile organic compound like benzene) through a porous medium, where it diffuses, is advected by pressure-driven groundwater flow, and undergoes first-order biodegradation. The governing equation for the contaminant concentration, $\phi(x,t)$, is given by:

$$\frac{\partial \phi}{\partial t} = \nabla \cdot (D_{\text{eff}}(x)\nabla\phi) - \nabla \cdot (\mathbf{v}_w(x)\phi) - k_{\text{bio}}(x)\phi$$

where:

- $\phi(x,t)$ is the concentration of the contaminant (mg/L).
- $D_{\text{eff}}(x)$ is the effective diffusion coefficient in the soil (mÂ²/s).

- $\mathbf{v}_w(x)$ is the groundwater velocity (m/s), influenced by the pressure gradient using the term: $(a(x)+1)^3\nabla p$.
- $k_{\text{bio}}(x)$ is the first-order biodegradation rate (1/s).
- $a(x) = \sin(2\pi x/L)$ is a spatially varying coefficient that influences both the diffusion and the velocity.

The pressure within the soil, $p(x,t)$, is coupled to the fluid flow and updated using a simplistic equation:

$$\frac{\partial p}{\partial t} = a'(x)\phi(x) + a''(x)$$

We employ a finite difference method to discretize the spatial domain and an implicit scheme for the time discretization, see [21] for such derivation. The key aspects of the method are:

- Spatial discretization: The domain $[0, L]$ is divided into Nx equal segments with grid spacing $\Delta x = L/(Nx-1)$.
- Implicit Time Discretization: An implicit scheme is used to update the value of ϕ at each time step.
- Laplacian operator: A finite difference discretization is used to form the Laplacian matrix.
- Pressure coupling: The gradient of pressure is computed with finite differences and used to updated the concentration.
- The pressure is updated using a simplified equation.

The simulation parameters are as follows:

- Soil Column Length: $L = 1$ m
- Number of Grid Points: $Nx = 100$
- Time Step: $\Delta t = 0.01$ s
- Total Simulation Time: $T = 1$ s
- Porosity: $\varepsilon = 0.4$
- Tortuosity: $\tau = 1.5$
- Molecular Diffusivity of benzene in water: $D_m = 1 \times 10^{-9}$ mÂ²/s
- Maximum Biodegradation Rate: $k_{\text{bio,max}} = 1 \times 10^{-6}$ 1/s
- Effective diffusion coefficient: $D_{\text{eff}} = \frac{\varepsilon D_m}{\tau}$
- Initial Condition: $\phi(x,0) = 0$, except for a constant value at the inlet. Initial pressure is set to zero.
- Boundary Conditions: Dirichlet boundary conditions are applied for both concentration and pressure: $\phi(0,t) = 5$, $\phi(L,t) = 0$, $p(0,t) = 0$, $p(L,t) = 0$.

The time-dependent behavior of the contaminant concentration, $\phi(x,t)$, and the pressure, $p(x,t)$, are presented in Figure 8, showing the transport,

diffusion, and biodegradation of the contaminant. This work has provided a framework for time-dependent simulations of contaminant transport in porous media, including the effect of pressure and biodegradation using an implicit method.

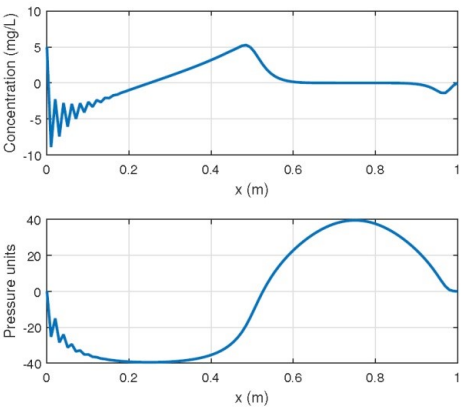

Figure 8

The concentration $\phi(x,t)$ and pressure within the solid material over time.

$$\frac{\partial \phi}{\partial t} = \nabla \cdot ((h_0 + a(x))^3 \nabla \phi) + \left(h_0 \frac{\partial \phi}{\partial x_1} + a'(x)\phi\right)$$

models the heat diffusion and advection in materials with spatially varying thermal properties. Here, $\phi(x,y,t)$ represents the temperature distribution, and $a(x)$ is a spatially varying property of the material, such as thermal conductivity or diffusivity. The term $(h_0 + a(x))^3$ represents the effect of the material's non-uniform thermal conductivity, which can vary due to composition, microstructure, or temperature.

5.2 Thermal Management in Heterogeneous Materials

This equation is particularly relevant for simulating heat transfer in heterogeneous materials or composite structures, where the material properties change spatially due to varying compositions or external conditions. For instance, in engine components or thermal insulation materials, the thermal conductivity often varies with location due to the presence of different materials, temperature gradients, or microstructural inhomogeneities. The diffusion term $\nabla \cdot ((h_0 + a(x))^3 \nabla \phi)$ models the heat conduction, while the advection term $h_0 \frac{\partial \phi}{\partial x_1} + a'(x)\phi$ accounts for any advective heat transport, which could arise from fluid motion in porous media or convective effects in materials. The equation we are dealing with is a two-dimensional parabolic PDE that models the evolution of a scalar field $\phi(x,y,t)$, which could represent a physical property such as temperature or concentration. The PDE is given by:

$$\frac{\partial \phi}{\partial t} = \nabla \cdot ((h_0 + a(x,y))^3 \nabla \phi) + \left(h_0 \frac{\partial \phi}{\partial x} + a'(x,y)\phi\right),$$

where:

- $\phi(x, y, t)$ is the scalar field representing the physical quantity: the temperature.
- For realistic simulations, material properties such as thermal conductivity may depend on temperature ϕ. You can use an empirical formula to model this dependence, such as:

$$a(x, y) = a_0(1 + \alpha(\phi(x, y) - \phi_0)),$$

where α is a material-dependent coefficient, $\phi(x, y)$ is the temperature at position (x, y), and ϕ_0 is a reference temperature.

- h_0 is a constant that scales the advection term.

We consider the following initial and boundary conditions for the problem:

- The initial distribution of $\phi(x, y, 0)$ is given by:

$$\phi(x, y, 0) = \sin\left(\frac{\pi x}{L_x}\right)\cos\left(\frac{\pi y}{L_y}\right).$$

This represents a temperature distribution that varies sinusoidally along both the x and y directions.

- Dirichlet boundary conditions are assumed, i.e., ϕ is fixed at the boundaries:

$$\phi(0, y, t) = \phi(L_x, y, t) = 0, \quad \phi(x, 0, t) = \phi(x, L_y, t) = 0.$$

This model is adapted for temperature-dependent conductivity, allowing for simulations where the thermal properties change as the material heats up, such as in high-performance heat exchangers, electronic cooling systems, or material testing under varying thermal loads. Figure 9 presents the evolution of the temperature in time t. As observed, the temperature distribution undergoes significant changes during the initial iterations, reflecting the transient nature of the heat transfer process. In the early stages, the system adjusts to the initial conditions and boundary effects, with temperature variations occurring rapidly across the domain. This is typical of systems where heat is being conducted and advected through materials with spatially varying properties. However, after a certain period, the temperature field stabilizes, and the rate of change diminishes. This stabilization is a result of the system reaching a dynamic equilibrium, where heat transfer has equilibrated across the domain, and the material's thermal properties, including the spatial variations in conductivity or diffusivity, have been fully incorporated into the solution. At this point, the temperature distribution becomes steady, and the thermal exchanges within the material become more realistic, resembling actual physical behavior. Figure 10 illustrates the steady-state temperature distribution within the microstructure after the system has stabilized. The left plot displays the temperature field as a smooth surface, with the jet colormap representing temperature variations (blue indicating lower temperatures and red indicating higher temperatures). The right plot provides a contour representation, highlighting temperature gradients across the domain. This visualization helps in understanding the thermal behavior and heat transfer within heterogeneous materials.

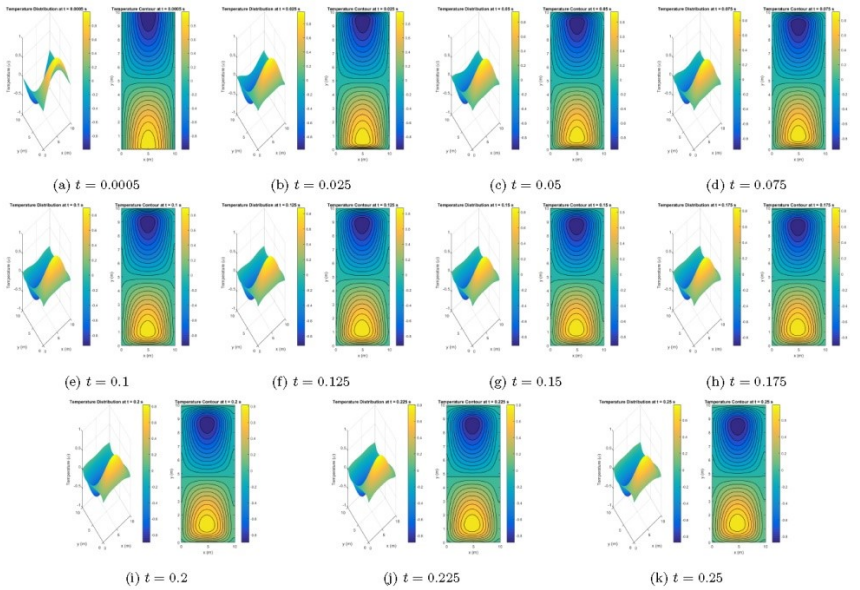

(a) $t = 0.0005$ (b) $t = 0.025$ (c) $t = 0.05$ (d) $t = 0.075$

(e) $t = 0.1$ (f) $t = 0.125$ (g) $t = 0.15$ (h) $t = 0.175$

(i) $t = 0.2$ (j) $t = 0.225$ (k) $t = 0.25$

Figure 9

Temperature Distribution and Contour Plot at different time. The color bar on both plots indicates the corresponding temperature scale in C.

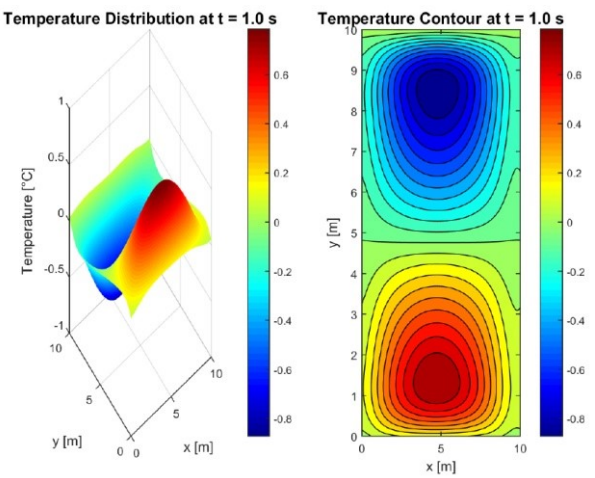

Figure 10

Final Temperature Distribution in the microstructure at time $t = 1.0$. The left plot shows the temperature distribution as a smooth surface, with the jet colormap indicating temperature variations (blue for cooler regions, red for hotter regions). The right plot presents the temperature contours, illustrating the spatial temperature gradients more clearly. The color bar on both plots indicates the corresponding temperature scale in C.

Conclusion

The study offers a comprehensive framework for modeling the dynamics of lubricated systems in the incompressible regime, emphasizing the interplay between the quasi-stationary Reynolds equation and Newton's second law. Through rigorous analysis of existence, uniqueness, and the conditions for the nonexistence of solutions, the paper establishes a solid theoretical foundation for further investigation into lubrication mechanisms. By proving the local uniqueness and existence of the solution $a(t)$, the work sets the stage for analyzing the system's temporal evolution. Moreover, the paper identifies specific conditions under which global solutions exist and outlines scenarios where global nonexistence occurs. Specifically, it demonstrates that for line contact ($\alpha \geq 2$), global existence is assured for all initial data and forces, whereas for certain ranges of α (particularly $\alpha \in]0,1[$), global nonexistence may arise when the applied force exceeds a critical threshold.

The results contribute significantly to the theoretical understanding of lubrication dynamics, offering valuable insights for practical applications. In particular, the numerical analysis underscores the crucial influence of parameters a and p on the system's behavior, providing essential guidance for optimizing lubrication designs in engineering contexts. Ultimately, this work advances the knowledge of lubrication dynamics, contributing to the development of more efficient and reliable lubrication systems across various industries, and paving the way for future advancements in lubrication technology.

Declarations

- **Ethical Approval:** Not applicable.
- **Funding:** Not available.

Conflict of interest

All the above authors approve that they don't have any conflict of interest.

Data availability

The datasets employed in this research can be obtained by contacting the corresponding author and submitting a reasonable request.

References

[1] I. Ciuperca, M. Jai, and J. I. Tello, “On the existence of solutions of equilibria in lubricated journal bearings,” *SIAM J. Math. Anal.*, vol. 40, no. 6, pp. 2316-2327 (Jan. 2009).

[2] U. Devani, J. Patil, S. Bilal, B. Hanumagowda, V. Trimbak, J. Tawade, N. Nazarova, and M. Gupta, “Study of MHD on porous flat and

curved circular plate lubricated with couple stress fluids—A slip velocity model," *Results Eng.,* vol. 24, p. 102914 (2024).

[3] I. El Malki, M. Alaoui, H. Mtai, and A. Laghrib, "Limitations of Chebyshev interpolation nodes: Counter examples and insights," *J. Interdiscip. Math.,* vol. 27, no. 3, pp. 575-600 (2024).

[4] S. Pfeil, H. Gravenkamp, F. Duvigneau, and E. Woschke, "Semi-analytical solution of the Reynolds equation considering cavitation," *Int. J. Mech. Sci.,* vol. 247, p. 108164 (2023).

[5] I. Hafidi, "An investigation of the singular perturbation problems for the compressible Reynolds equation," *Differ. Integral Equations,* vol. 22, no. 1/2 (Jan. 2009).

[6] T. Jiang, D. Nie, and J. Lin, "Swimming velocity of spherical squirmers in a square tube at finite fluid inertia," *Appl. Math. Mech.*, vol. 45, no. 9, pp. 1481-1498 (2024).

[7] A. Karniadakis and Beskok, Microflows and Nanoflows, *Interdiscip. Appl. Math.* (2005).

[8] M. Ibtesam, S. Nadeem, and J. Alzabut, "Numerical computations of magnetohydrodynamic mixed convective flow of Casson nanofluid in an open-ended cavity formed by earthquake-induced faults," *Appl. Math. Mech.*, vol. 45, no. 12, pp. 2215-2230 (2024).

[9] S. Kistler, Liquid Film Coating, Springer Netherlands (1997).

[10] M. Marian and S. Tremmel, "Physics-informed machine learning—an emerging trend in tribology," *Lubricants,* vol. 11, no. 11, p. 463 (Oct. 2023).

[11] J. B. Grotberg and O. E. Jensen, "Biofluid mechanics in flexible tubes," *Annu. Rev. Fluid Mech.,* vol. 36, no. 1, pp. 121-147 (Jan. 2004).

[12] M. Srati, A. Oulmelk, L. Afraites, A. Hadri, M. A. Zaky, and A. Hendy, "Learning primal-dual approach for space-dependent diffusion coefficient identification in fractional diffusion equations," *J. Comput. Phys.,* vol. 523, p. 113646 (2025).

[13] Y. Cheng, Q. He, W. Huang, Y. Liu, Y. Li, and D. Li, "HL-Nets: Physics-informed neural networks for hydrodynamic lubrication with cavitation," *Tribol. Int.,* vol. 188, p. 108871 (Oct. 2023).

[14] G. Buscaglia, I. Ciuperca, I. Hafidi, and M. Jai, "Existence of equilibria in articulated bearings," *J. Math. Anal. Appl.*, vol. 328, no. 1, pp. 24-45 (Apr. 2007).

[15] I. I. Ciuperca and M. Jai, "Singular perturbation problem for the incompressible Reynolds equation," *Electron. J. Differ. Equ.*, vol. 83, no. 1/2 (2006).

[16] W. Boscheri, A. Chiozzi, M. G. Carlino, and G. Bertaglia, "A new family of semi-implicit finite volume/virtual element methods for incompressible flows on unstructured meshes," *Comput. Methods Appl. Mech. Eng.,* vol. 414, p. 116140 (2023).

[17] S. Saha, P. Biswas, and S. Nath, "Bifurcation phenomena for incompressible laminar flow in expansion channel to study Coanda effect," *J. Interdiscip. Math.*, vol. 23, no. 2, pp. 493-502 (2020).

[18] Z. Peng and K. Iwamura, "A sufficient and necessary condition of uncertainty distribution," *J. Interdiscip. Math.*, vol. 13, no. 3, pp. 277-285 (2010).

[19] C. Cendon, "Existence and uniqueness of solution for a lubrication problem with cavitation in a journal bearing with axial supply," *Adv. Math. Sci. Appl.,* vol. 14, no. 1, pp. 313-331 (1994).

[20] J. I. Diaz and J. I. Tello, "A note on some inverse problems arising in lubrication theory," *Differ. Integral Equations,* vol. 17, no. 5-6 (Jan. 2004).

[21] F. J. Profito, M. Giacopini, D. C. Zachariadis, and D. Dini, "A general finite volume method for the solution of the Reynolds lubrication equation with a mass-conserving cavitation model," *Tribol. Lett.,* vol. 60, pp. 1-21 (2015).

[22] L. Van Hoecke, D. Boeye, A. Gonzalez-Quiroga, G. S. Patience, and P. Perreault, "Experimental methods in chemical engineering: Computational fluid dynamics/finite volume method—CFD/FVM," *Can. J. Chem. Eng.,* vol. 101, no. 2, pp. 545-561 (2023).

[23] M. Alahyane, A. Hakim, A. Laghrib, and S. Raghay, "Fluid image registration using a finite volume scheme of the incompressible Navier-Stokes equation," *Inverse Probl. Imaging*, vol. 12, no. 5 (2018).

[24] M. Rahman, "Compromising with corrector step of simple algorithm," *Math. Comput. Simul.,* vol. 188, pp. 135-163 (2021).

[25] K. R. Raghunatha and S. Kumbinarasaiah, "Laguerre wavelet numerical solution of micropolar fluid flow in a porous channel with high mass transfer," *J. Interdiscip. Math.,* vol. 24, no. 8, pp. 2269-2282 (2021).

Received March, 2025